Exceptionally Stable Cobalt Nanoclusters on Functionalized Graphene

Valeria Chesnyak, Srdjan Stavrić, Mirco Panighel,* Daniele Povoledo, Simone del Puppo, Maria Peressi, Giovanni Comelli, and Cristina Africh

To improve reactivity and achieve a higher material efficiency, catalysts are often used in the form of clusters with nanometer dimensions, down to single atoms. Since the corresponding properties are highly structure-dependent, a suitable support is thus required to ensure cluster stability during operating conditions. Herein, an efficient method to stabilize cobalt nanoclusters on graphene grown on nickel substrates, exploiting the anchoring effect of nickel atoms incorporated in the carbon network is presented. The anchored nanoclusters are studied by in situ variable temperature scanning tunneling microscopy at different temperatures and upon gas exposure. Cluster stability upon annealing up to 200 °C and upon CO exposure at least up to 1×10^{-6} mbar CO partial pressure is demonstrated. Moreover, the dimensions of the cobalt nanoclusters remain surprisingly small (<3 nm diameter) with a narrow size distribution. Density functional theory calculations demonstrate that the interplay between the low diffusion barrier on graphene on nickel and the strong anchoring effect of the nickel atoms leads to the increased stability and size selectivity of these clusters. This anchoring technique is expected to be applicable also to other cases, with clear advantages for transition metals that are usually difficult to stabilize.

V. Chesnyak, S. Stavrić, D. Povoledo, S. del Puppo, M. Peressi, G. Comelli
Physics Department
University of Trieste
via A. Valerio 2, 34127 Trieste, Italy

V. Chesnyak, M. Panighel, G. Comelli, C. Africh
CNR - Istituto Officina dei Materiali (IOM), Trieste, Laboratorio TASC
Strada Statale 14, km 163.5, Basovizza, 34149 Trieste, Italy
E-mail: panighel@iom.cnr.it

S. Stavrić
Vinča Institute of Nuclear Sciences – National Institute of the Republic of Serbia
University of Belgrade
P. O. Box 522, RS-11001 Belgrade, Serbia

M. Peressi
ICSC - Italian Research Center on High Performance Computing
Big Data and Quantum Computing
40033 Casalecchio di Reno (Bologna), Italy

The ORCID identification number(s) for the author(s) of this article can be found under https://doi.org/10.1002/sstr.202400055.

1. Introduction

Supported metal clusters are widely used in heterogeneous catalysis,[1] electrocatalysis,[2,3] as well as spintronics and magnetic storage devices.[4–6] All these applications rely on the structure-dependent properties of both the clusters and the support. More specifically, the clusters' active sites strongly depend on the specific reaction mechanism,[7] while a precise cluster size selectivity is crucial as a difference of just one atom can drastically affect the reactivity.[8–10] When it comes to operation in realistic conditions, such as high temperatures and/or exposure to reactants,[11–13] the clusters may also suffer from restructuring and sintering, eventually leading to their deactivation. A suitable support may help by offering adsorption sites capable of enhancing the stability of clusters.[14,15] In this respect, carbon-based materials like graphene (G) exhibit additional desirable properties such as mechanical strength, conductivity, possibilities for functionalization and chemical inertness,[16] outperforming other supports.[17,18] However, stabilizing metal clusters on such supports poses similar stability challenges that need to be addressed. Furthermore, it should be noted that the structure and properties of the clusters strongly vary depending on the nature of their atomic components: their size, for instance, strongly depends on the cohesive energy of the constituting metal, as in general the lower the cohesive energy, the larger the particle size.[19] In addition, the support not only can act as a stabilizer for the clusters but may also affect their catalytic activity.

The most common approach for stabilizing small clusters is to grow them at low temperatures,[20] often exploiting the templating effect of a moiré modulated support, as the one resulting from the lattice mismatch between G and the underlying substrate.[19,21] However, this approach cannot be used for many catalytic reactions that take place at elevated temperatures, and thus is not suitable for industrial applications. Alternative ways to anchor small clusters and maintain their structure have been proposed. For instance, it has been demonstrated that the adsorption of radicals prevented coarsening[22] while seeding by high cohesive energy metals provided nucleation sites for low cohesive energy metals.[19] However, these methods require additional steps in the fabrication process and, moreover, they are likely

to alter the chemical nature of the clusters. Other methods involve the functionalization of the G support, for example, by introducing vacancies or heteroatoms directly into the layer, which results in an increased cluster stability with respect to the pristine G layer.[23–25] Furthermore, heteroatoms inserted in the G network not only stabilize the clusters' structure but are also predicted to enhance their carbon monoxide (CO) adsorption capability.[26,27] Finally, single-atom catalysts were recently proposed as templating structures for cluster growth.[28]

This study presents an extensive experimental and theoretical investigation of supported cobalt (Co) clusters and their stability upon annealing and exposure to CO. Co is deposited on G grown on nickel (Ni) and characterized by variable-temperature scanning tunneling microscopy (VT-STM) and density functional theory (DFT). The choice of substrates used, namely, Ni(111) and Ni(100), has a twofold motivation. On the one hand, it allows to clarify the possible effect of the specific surface orientation and the presence of a moiré structure on the stability of the metal clusters; on the other hand, since these are the most abundant crystallographic orientations in polycrystalline Ni foils,[29] it provides a perspective of scaling up our results beyond model systems toward more realistic applications.

To investigate their stability, the Co clusters are annealed until they undergo a substantial structural change; furthermore, their invariance upon exposure to reactants is investigated by in situ STM measurements at different CO gas pressures. DFT simulations were performed to shed light on the origin of the clusters' structure and stability, calculating the binding energies and diffusion barriers of Co atoms on G. Overall, an efficient method to stabilize nanometer-sized Co clusters, based on the incorporation of individual Ni atoms in the G network, is described. This method is potentially transferrable to other metal clusters and Ni substrates, opening the way for synthesizing tailored systems to investigate reactions from the fundamentals toward the industrial scale.

2. Results and Discussion

2.1. Structure and Characterization at Room Temperature

Clusters were formed after the deposition of Co on G grown on Ni(111)[30] and Ni(100).[29] The main difference between the two supports is the corrugation of the G layer, as on Ni(111) it remains flat and epitaxial while on Ni(100) it is corrugated in a stripe-like fashion, due to the unmatching symmetry of the sixfold G and the fourfold Ni(100) substrate.[31,32] In the latter case, one distinguishes between high-interacting, chemisorbed sites (valleys) and low-interacting, physisorbed sites (ridges).[33] On both substrates, a remarkable common feature (yet more favored on Ni(111)) is the incorporation of individual Ni atoms, which remain trapped within the G mesh during growth.[34] The respective G layers before Co deposition are presented in Figure S1, Supporting Information.

After Co deposition, spherical, bright protrusions, randomly distributed on both substrates, are visible in the STM images (see **Figure 1**) and are easily attributed to Co clusters (see Figure S1, Supporting Information, for comparison without Co clusters). Two significant features are immediately noticed: 1) at room temperature, these Co clusters remain immobile on both supports, irrespective of the presence of a moiré structure; 2) their typical size is considerably smaller in comparison to previous studies on similar systems.[4,19,35–37] The insets show that the smallest observed species related to Co are in both cases single adatoms and dimers. Cluster densities are describing the number of clusters in a certain area of interest. Cluster sizes were always estimated using the highest point of the cluster to obtain the height distribution and the whole peak area to extract the diameter, a simplified procedure that leads to an overestimation but still is useful for a systematic comparison. The detailed procedure is demonstrated through an example in Figure S2, Supporting Information. All reported cluster sizes throughout the text are summarized in **Table 1**. On the epitaxial G/Ni(111) support, clusters appear to be small, with average sizes,
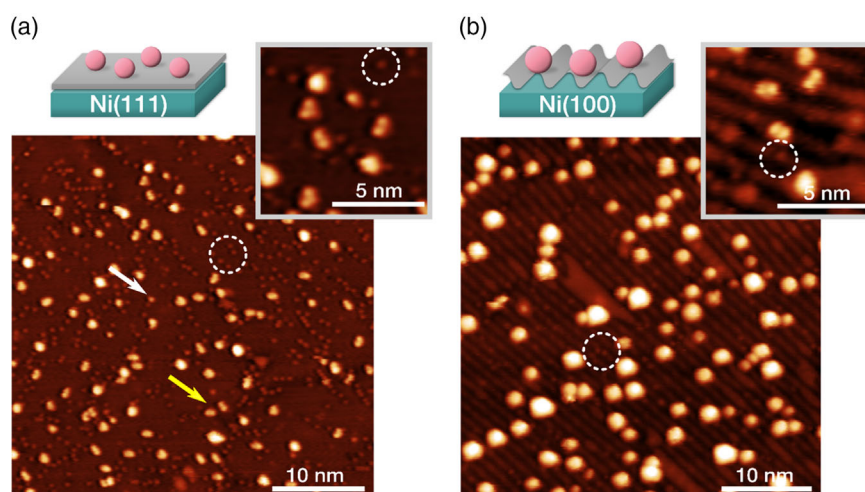

Figure 1. a) Room temperature STM images of Co clusters deposited on G grown above Ni(111), and b) above Ni(100) as illustrated in the schematic models. Insets in (a) and (b) show high-resolution STM images of the smallest cluster species observed, corresponding to dimers (yellow arrow) and single adatoms (white arrow). White dashed circles highlight substitutional Ni atoms in G, observed in both samples. (a, inset: $I_t = 0.6$ nA, $V_b = -1.0$ V, b: $I_t = 0.3$ nA, $V_b = -1.1$ V, inset: $I_t = 0.3$ nA, $V_b = -1.0$ V).

Table 1. Summary of all the cluster sizes obtained upon different conditions presented in this study. The detailed procedure for size estimation is described in Figure S2, Supporting Information. The maximum sizes were obtained from line profiles across the largest clusters.

System	Average diameter (maximum diameter) [nm]	Average height (maximum height) [nm]	Coverage, conditions
Co/G/Ni(111)	1.4(2.5)	0.2(0.5)	0.03 ML, R.T.
Co/G/Ni(100)	2(4)	0.5(1.5)	0.03 ML, R.T.
Co/G/Ni(111)	1.6	0.5	0.03 ML, 200 °C
Co/G/Ni(100)	2.5	0.6	0.03 ML, 200 °C
Co/G/Ni(111)	2.4	0.6	0.21 ML, R.T.

Table 2. Comparison of the observed cluster size ranges of this study (Co/G/Ni(111) and Co/G/Ni(100)) and those reported in the literature. R.T. Refers to room temperature during Co evaporation/measurement. Coverage and special stabilization technologies are specified.

System	Diameter range [nm]	Height range	Coverage, conditions, details	Reference
Co/G/Ni(111)	0.8–2.5[a]	0.2–0.5 nm	0.03 ML, R.T.	This work
Co/G/Ni(100)	0.8–4[a]	0.2–1.5 nm	0.03 ML, R.T.	This work
Co/G/Ir(111)	2.5–30[b]	up to 3 nm	0.25–>1 ML, R.T., seeding technology by Pt, Ir	[4]
Co/G/Ru(0001)	10[c]	–	0.2 ML, R.T.	[35]
Co/HOPG(graphite)	2–14	0–3 nm	0.13–0.43 ML, R.T.	[36]
Co/G/SiC(0001)	5–9	0.4–1.2 nm[b]	0.13–0.26 ML, R.T.	[36]
Co/G/SiC(0001)	up to 10[c]	0.1–0.6 nm	0.02 ML, R.T.	[37]
Co/G/Ru(0001)	1.7–6.24	0.3–3 nm	0.13–2.5 ML, R. T.	[38]

[a]Size of a single Co adatom: 0.8 nm width and 0.2 nm height. [b]Increase in size with increasing coverage of Co. [c]Rough estimation from presented STM image.

estimated from over 200 clusters, of about 1.4 nm in diameter and 0.2 nm apparent height, compatible with a two-dimensional structure, with the largest ones reaching 2.5 nm width and 0.5 nm height. On the corrugated G/Ni(100) support, shown in Figure 1b, the observed nanoclusters are slightly larger, exhibiting an average height of 0.5 nm and 2.0 nm in diameter, estimated from over 600 clusters (largest clusters are up to 1.5 nm high and 4 nm wide). The slightly increased size with respect to the G/Ni(111) support will be addressed further in Section 2.2. Besides the Co structures, the STM images reveal the presence of doping Ni atoms trapped inside the G layer, visible as smaller and less bright protrusions for both G layers (encircled in dashed white in Figure 1).

It is important to underline that in both cases the clusters' dimensions are considerably smaller than previously reported for other substrates. Indeed, on other G supports, when no seeding technologies are used, Co usually forms sparse nanoparticles of larger dimensions,[4,19,35–37] mainly due to low G–Co interaction and rather high Co—Co bond strength. Previous studies on Co/G/Ru(0001) find species with dimensions ranging from 1.7 nm average diameter on moiré-modulated G, up to more than 10 nm with increasing coverage.[35,38] A comparison of the sizes observed in this study with those previously reported in literature on other supports or with different stabilization methods is reported in **Table 2**.

2.2. Origin of the Cluster Anchoring and Stabilization

The main point of interest at this stage is the origin of the clusters' stability provided by the support. At variance with previous works, the Co nanoclusters obtained in this case are stable at room temperature, irrespective of the presence of a templating moiré structure, therefore indicating the existence of another stabilizing factor. To identify the origin of the stabilization, we removed the clusters and exposed their adsorption sites, thanks to the atomic manipulation capabilities of the STM. As illustrated by the model in **Figure 2**a, the STM tip was moved closer to the clusters during the scan (by increasing the tunneling current up to 3.5 nA and reducing the bias voltage to 30 mV), to induce their displacement. The area before the removal is imaged in Figure 2b,c for G/Ni(111) and G/Ni(100), respectively. After the manipulation procedure, the tip was retracted to normal

scanning conditions, revealing in the cleared area the adsorption sites on the two supports (Figure 2e,f). To reconstruct the exact position of the clusters, the two images, before and after the manipulation, are superimposed in Figure 2h,i, where the silhouettes of the clusters mark their initial positions. Without any exception, both support the removal of Co clusters by the tip manipulation uncovers the presence of Ni atoms incorporated in the G layer, showing that they function as efficient anchoring sites for Co atoms and clusters, and providing a likely explanation for the observed stability.

As previously reported, the concentration of Ni atoms trapped in the G mesh is not homogeneous[34] but depends on several factors, e.g., the rotational domain of the G flake and the specific growth mechanism, which in turn is affected by parameters such as substrate temperature, pressure of precursor gas, and C precontamination in the subsurface.[33] Typically, a lower growth temperature and a longer growth time favor a high concentration of incorporated Ni atoms. In the current work, we confirm a non-homogeneous distribution of Ni dopants in the layer (Figure S1, Supporting Information), which well explains the observed different densities, i.e., the number of Co clusters in adjacent G flakes, visible in Figure S3, Supporting Information, further supporting the anchoring role of the Ni dopants. Consequently, as the deposited amount of Co has to be distributed to fewer Ni dopants in such regions, the average cluster size is expected to be larger with respect to G/Ni(111), as actually observed in Figure 1b. Furthermore, the deposition of 0.03 monolayer (ML) of Co leaves many unoccupied Ni anchors in the G layers on both substrates, particularly for G/Ni(111). Deposition of an additional 0.18 ML of Co (1 h and 10 min and 0.21 ML in total) leads to the formation of new clusters anchored to the unoccupied dopants but, surprisingly, to only a marginal increase of the average cluster size (2.4 nm width, 0.6 nm height estimated for over 200 clusters). A representative STM image of the higher coverage is shown in Figure S3, Supporting Information. Therefore,
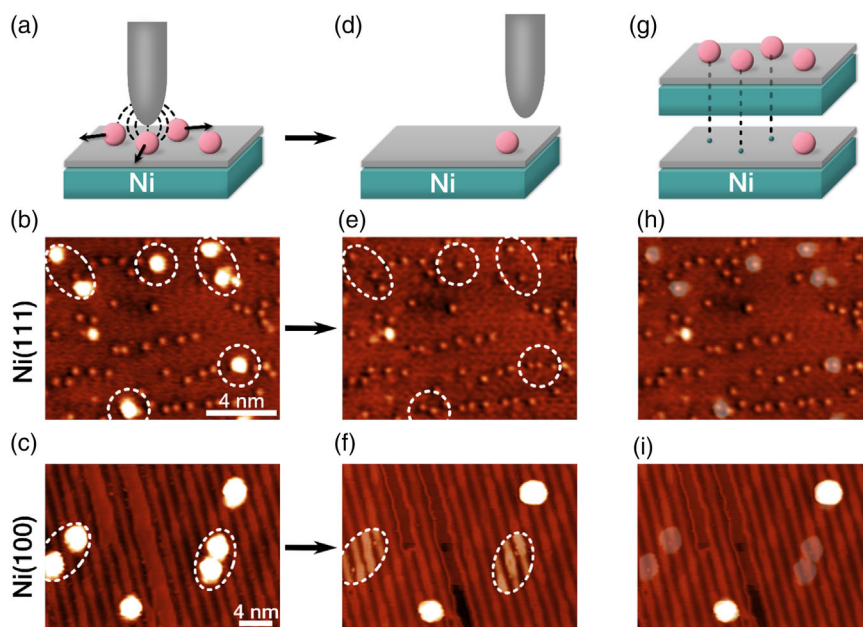
Figure 2. Revealing the cluster adsorption site by STM manipulation. a,d) Schematic of the Co clusters manipulation. b) STM images of Co clusters (encircled) on G/Ni(111) and c) G/Ni(100) before manipulation. STM images of the same areas in e,f) show the surfaces after removal of Co clusters and the respective adsorption sites, encircled and contrast adjusted in (f) for the sake of visibility of the Ni atoms. h,i) Superposition of the STM images before and after manipulation to reconstruct the exact position of the removed clusters, as illustrated in scheme g). (b: $I_t = 0.5$ nA, $V_b = -2.0$ V, c: $I_t = 0.3$ nA, $V_b = -0.7$ V, e: $I_t = 3.5$ nA, $V_b = -2.0$ V, f: $I_t = 0.3$ nA, $V_b = -0.7$ V).

we conclude that the growth of existing clusters becomes less favorable upon reaching a certain size. This aspect will be further elucidated in Section 2.3 and 2.4, where we present a more detailed analysis using DFT and investigating the thermal stability, respectively.

In short, the experimental results indicate that the Ni atoms incorporated in the G mesh act as anchors for the Co nanostructures, that otherwise on a pristine, defect-free G would be unstable at room temperature on both Ni substrates. It can be further ruled out that the clusters are stabilized by vacancies that later are occupied by Co atoms, as they are not present in the layer before Co deposition. An exchange mechanism between the Co atoms of the cluster and the Ni dopant inside G is highly unlikely due to the high stability of the Ni—C bond and the additional interaction between the Ni dopant and the underlying Ni substrate.[34,39] The fact that we observe even the smallest species, namely, adatoms and dimers, and relatively small nanoclusters as the largest structures, suggests a high binding energy between Co and the Ni anchor, as adsorbed Co typically tends to stabilize in larger structures.[4,19,35–37] To investigate this issue, we performed DFT calculations, which are reported in the following section.

2.3. DFT Calculations

We performed DFT calculations for single Co adatoms and small nanoclusters both on valleys and ridges of the G/Ni(100) substrate. It is worth to note that the results obtained for the valley case can be reasonably extended to the G/Ni(111) case, as the binding of valleys on Ni(100) is very similar to G binding on Ni(111).

The growth morphology of clusters on supports of this kind is typically affected by a convolution of thermodynamic and kinetic parameters, such as 1) the adsorption energy between the adsorbed species and the adsorption site; 2) the diffusion barrier across the support; 3) the incremental binding energy between the adsorbed species (i.e., the energy gain as a result of the addition of a Co atom to an adsorbed Co structure; 4) the Ehrlich–Schwöbel barrier (Co hopping barrier on the first layer yielding three-dimensional structures instead of two-dimensional ones), and 5) the strength of the G-substrate interaction and possible charge transfer from the substrate to G, as it can decrease the interaction between the deposited metal and G.[19,35,36,40]

In ref. [41], we defined the adsorption energy per atom of a cluster composed of n Co atoms with respect to the substrate and the free atoms as:

$$E_{ads}(n) = \frac{1}{n}\left(E_{Co_n/substrate} - nE_{Co} - E_{substrate}\right) \tag{1}$$

where $E_{Co_n/substrate}$, E_{Co}, and $E_{substrate}$ are the total energies of the whole system, of an isolated free Co atom and of the substrate (we extend this definition here including the Ni atom inside the double vacancy), respectively. This definition gives a negative intensive quantity (eV atom^{-1}).

We first analyze the behavior of an individually adsorbed atom. The calculated E_{ads} for a Co atom at the anchor on the valley is -2.43 eV, whereas the adsorption is slightly stronger on the ridge, yielding the E_{ads} of -2.59 eV (**Figure 3**, position no. 1). For comparison, the adsorption of a Co adatom on the pristine G valley and ridge is much weaker, quantified with E_{ads} of

**ADVANCED
SCIENCE NEWS**

www.advancedsciencenews.com

small
structures
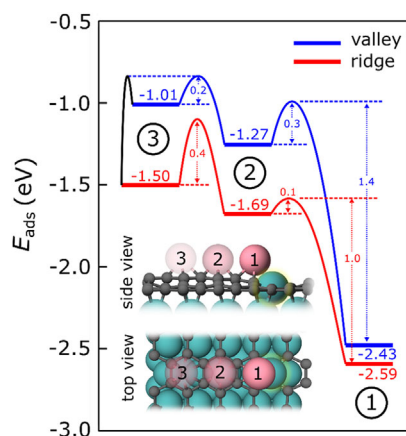
www.small-structures.com

Figure 3. Energetics (adsorption energies and barriers) of a single Co atom moving along paths on valleys (blue) and ridges (red) of G/Ni(100), starting from a hollow site far from the anchor (no. 3, left) and reaching a Ni-passivated double vacancy (no. 1, right). The black line on the left indicates the diffusion barrier between the valley and the ridge. The intermediate position (no. 2, center) corresponds to a hollow site close to the defect. The ball-and-stick model (side and top view) sketches the diffusion path of a Co adatom along the ridge: transparent pink spheres indicate the initial, intermediate, and final positions along this path.

-1.01 and -1.50 eV, respectively.[41] Therefore, anchoring a single Co adatom diffusing on the surface reduces the total energy of the Co/G/Ni(100) system by at least ≈ 1 eV, depending on the adsorption site from where the Co adatom started its diffusion. Remarkably, the DFT results shown in Figure 3 indicate that the strong difference in the adsorption energy between the valley and the ridge far from the defect (≈ 0.5 eV) reduces to only 0.16 eV at the anchor. This implies that the effect of the anchor is much more relevant than the electrostatic repulsion between the Co adsorbate and the Ni support on valleys discussed in ref. [41].

Coming to the Co diffusion, the barriers for the displacement of a single Co adatom from the nearest G hollow site to the Ni anchor were calculated by means of the nudged elastic bands (NEB) method. The rather low barriers we obtained –0.3 eV (valley) and 0.1 eV (ridge) – prove that Co atoms can easily approach the Ni anchor from neighboring G sites (Figure 3). The opposite movement away from the anchor requires overcoming much higher barriers –1.4 eV (valley) and 1.0 eV (ridge) – clearly showing that the Co atoms, once anchored, cannot easily detach. For comparison, Figure 3 also includes the diffusion barriers far from the anchor, giving a complete overview of the possible anchoring paths along valleys and ridges and across them.[41]

Coming to multiatomic clusters, E_{ads} (shown in Figure S4, Supporting Information, for the most stable structures of Co_n for n ranging from 1 to 4) in absolute value increases with the number of atoms. To rationalize the growth mode of Co clusters, we define the incremental binding energy, δE_{bind}, as the (positive) energy gain when a Co atom is sequentially added from the gas phase to an already formed adsorbed cluster. For the additional n-th atom ($n \geq 2$, in terms of total energies of the adsorbed Co_n and Co_{n-1} clusters and of an isolated Co, the incremental binding energy is therefore:

$$\delta E_{bind}(n) = E_{Co_{n-1}/substrate} + E_{Co} - E_{Co_n/subsate} \qquad (2)$$

which is related to E_{ads} as follows:

$$\delta E_{bind}(n) = nE_{ads}(n) - (n-1)E_{ads}(n-1) \qquad (3)$$

In other words, δE_{bind} is related to the differential heat of adsorption, as for example, measured by Campbell's group and compared with DFT predictions for other metallic clusters on G/Ni(111).[42] In **Figure 4**, we show δE_{bind} calculated both with (central panel) and without anchoring (left panel), for comparison. The calculated anchored Co structures are depicted in Figure 4c (clusters on valley) and d (clusters on ridge).

It is evident that δE_{bind} with and without anchoring for the inspected multiatomic clusters such as Co_4 does not differ so much, suggesting that the effect of the anchor is very strong for the first atom but reduces for the additional ones. However, δE_{bind} globally shows an increasing trend with the cluster size, reaching values of about 4 eV for the most favored inspected structures (three-dimensional for Co_4). Consequently, it is convenient for Co to start clustering. Furthermore, the fact that the inspected three-dimensional clusters are more stable than two-dimensional ones, as the Co–Co bonds are much stronger than the bond of Co to G, suggests the presence of a small Ehrlich–Schwöbel barrier. This conclusion is corroborated by experimental STM images that show many three-dimensional Co structures.

Due to high computational demands, our calculations are necessarily limited to clusters containing very few atoms. However, the behavior of $E_{ads}(n)$ (Figure S4, Supporting Information) and $\delta E_{bind}(n)$ (Figure 4) both approaching a saturation value with the number of atoms n, suggests that, while clusterization is initially strongly favored, it is not necessarily so when cluster size increases, due to opposing contributions. For instance, as previously reported,[41] the strong interaction of G on Ni leads to an electronic charge transfer to the G layer and thus results in n-doped G, which is known to weaken the bonding with the deposited metal. This also explains why on the G/Ni(111) support, where the G to Ni interaction is strong and comparable to the valley regions on Ni(100), the Co nanoclusters are less stable, and the anchoring effect of the Ni atom incorporated into the G network becomes even more relevant.

At this point, the structure, the small size, and the remarkable stability of the observed Co structures are well understood. Since this Ni-doped G support represents a new class of cluster stabilization methods and its potential application in catalysis is very promising, it is important to investigate the temperature and pressure stability of this system. For this reason, in situ STM experiments were conducted upon annealing and gas exposure of Co clusters on Ni-doped G.

2.4. Temperature Stability

As the role of clusters in catalysis relies on the specific reactivity dictated by their small size, a fundamental requirement is the preservation of this specific structure and size at operating conditions. To determine their stability, we investigated the behavior of the Co clusters at elevated temperatures and upon contact with reactants, i.e., during gas exposure. Temperature-induced
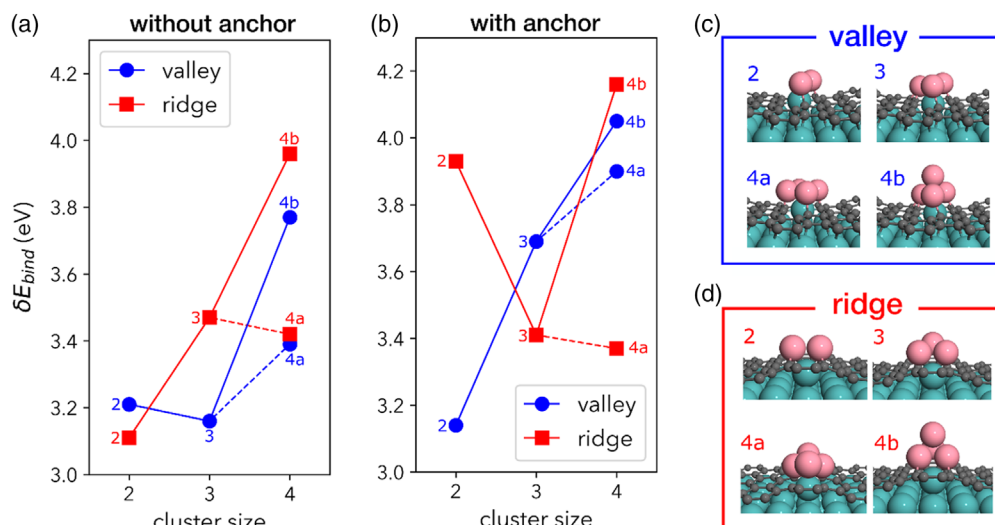
Figure 4. Incremental binding energy as a function of cluster size for Co clusters on G valleys (blue) and ridges (red): a) clusters on defect-free G/Ni(100); b) clusters anchored at the substitutional Ni-anchor inside a double vacancy. The panels on the right show the ball-and-stick configurations for the anchored clusters on c) valleys and d) ridges.

structural changes were studied by annealing the samples up to 300 in 50 °C steps, acquiring STM images at each step. Selected images are shown in **Figure 5**. The Co clusters at 200 °C for the G/Ni(111) and G/Ni(100) surfaces are displayed in Figure 5a,c, respectively. Compared to the room temperature measurements, the clusters are more uniform in size, while remaining rather

Figure 5. STM images of Co nanoclusters on G/Ni(111) (left) and G/Ni(100) (right) measured in situ at increasing temperatures: a,c) 200 °C, b) 250 °C, and d) 300 °C, showing that only at 250 °C on G/Ni(111) and 300 °C on G/Ni(100) the cluster density decreases and ripening/intercalation sets in. (a: $I_t = 0.4$ nA, $V_b = -2.0$ V, b: $I_t = 0.4$ nA, $V_b = -1.0$ V, c: $I_t = 0.2$ nA, $V_b = -1.83$ V, d: $I_t = 0.2$ nA, $V_b = -1.0$ V).

small and stable. Their average dimensions on G/Ni(111) increase to 1.6 nm in diameter and 0.5 nm in height (estimated from 169 clusters) while on G/Ni(100), they remain similar to the room temperature case, 2.5 nm in diameter and 0.6 nm in height (estimated from 64 clusters). Furthermore, while usually annealing leads to the broadening of the cluster size distribution until intercalation sets in ref. [43], in the present case, we observe a remarkably sharper size distribution. STM time series shows that at this temperature clusters retain their configuration for at least 30 min on both supports.

Upon annealing to a higher temperature, the Co nanoclusters on G/Ni(111) mostly vanish at 250 °C through dissociation and diffusion, followed by intercalation at the interface between G and Ni(111), as indicated by the appearance of two-dimensional islands of monoatomic height, as shown in Figure 5b, similarly to what previously observed at 200[38] and 527 °C,[44] also on other supports. In contrast, on the G/Ni(100) support, at 250 °C the Co structures are still stable, while a significant reduction of the clusters' density, likely due to their intercalation, is observed only at 300 °C (see Figure 5d). The additional stabilization arises from the stripy corrugation, as shown by the calculated E_{ads} ∨, higher on the ridges than on the valleys (the latter representative also of G/Ni(111)). Therefore, the corrugation of the layer plays a role—in addition to the Ni anchor—for Co stabilization, resulting in a ≈50 °C higher temperature stability on the G/Ni(100) support.

Although we do not provide a direct computational justification for the observed maximal size of Co clusters, some hints can be inferred from our calculations for the few-atom clusters, based on the interplay between the strong interaction the Co atoms establish near the anchor and the repulsion they feel from the strongly interacting, chemisorbed regions of G on the Ni substrate. As a consequence, a few-atom cluster can be significantly stabilized by the Ni anchor, while further growth involves atoms that experience increasingly weaker anchoring until the repulsive interaction with the G/Ni support outweighs the anchoring
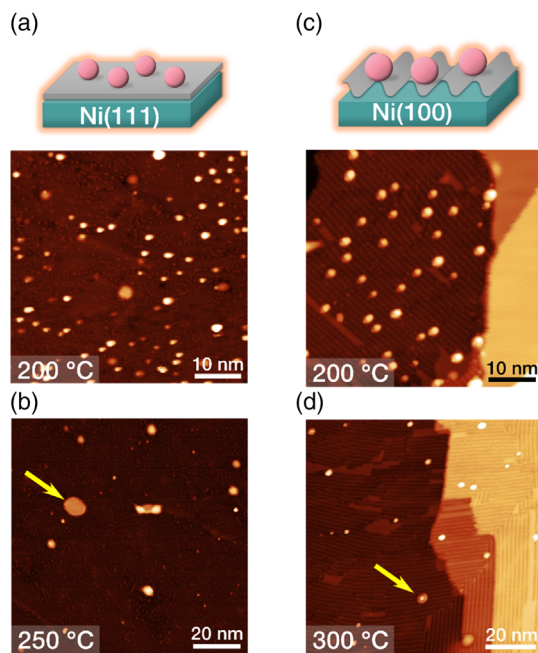
forces. This results in a self-limiting size mechanism, as additional Co atoms are less likely to attach to larger clusters, preferring instead smaller clusters or naked Ni anchors. Upon annealing, the less stable structures, such as single atoms and dimers, undergo Ostwald ripening and attach to already-formed clusters until a critical size is reached when further enlargement becomes unfavorable. Under equilibrium conditions, the cluster dimension distribution sharpens and the system naturally undergoes sort of a size selection.

2.5. Pressure Stability

The second aspect worth investigating is the behavior of the supported Co clusters upon exposure to potential reactants. We chose to focus on the G/Ni(100) support, this facet being the most abundant in polycrystalline Ni surfaces,[29] expecting again to similarly extend the results to G/Ni(111). It is well known that in general CO can induce mass transport with huge effects on the structure of the catalyst.[11,45–48] At the same time, this molecule is present in many reactions which involve Co as a catalyst.[49,50] To investigate the stability of Co clusters on G/Ni(100) upon gas adsorption, the system was exposed to CO at room temperature, while imaging in situ by STM. The same area before and after 90 min CO exposure of ≈ 1500 L in total, (sequence of 30 min exposure at increasing pressures, 1×10^{-7}, 3.3×10^{-7}, and 1×10^{-6} mbar) is shown in **Figure 6**a,b, respectively. No structural change is observed under these conditions: the Co clusters remain at their position, with the same structure and size and even clusters close to each other do not merge. The observed structural stability, though, does not imply that the cluster remains inert. Indeed, although the image acquisition time of

40 s/frame prevents the observation of fast dynamics, during the exposure some clusters become suddenly brighter, typically reverting to their initial size and shape in the subsequent frame. The whole movie of the acquired sequences can be appreciated in ref. [51] while selected frames are presented in Figure S5, Supporting Information. We attribute this random blinking of the Co clusters to a fast adsorption-desorption process,[47] which would require further investigation to be confirmed, out of the scope of the present work. Explanation of the effect as due to tip-induced interactions can be ruled out since it was not observed in the absence of the gas. This result is promising for further studies toward a real catalytic application of this system. Indeed, this system meets the requirements for a wide range of relevant catalytic reactions taking place up to 200–250 °C, such as the Fischer–Tropsch reaction,[9,52–55] selective CO_2 hydrogenation,[56,57] oxidative dehydrogenation,[58] and ammonia dehydrogenation.[23] It is worth noting that the absence of a long-range order of the clusters can be limiting for some specific techniques or applications, whereas, for catalytic purposes at the active sites of the single cluster, it should not play a role. Furthermore, there are studies suggesting that larger nanoclusters and particles that meet the size selection provided by this system, favor specific reaction mechanisms.[8,10,59] In addition, with such a uniform cluster size, this system is suitable for investigating reaction mechanisms at the atomic scale using spectroscopic methods.[60] Finally, besides clusters' stabilization, the Ni anchors might play an additional role in catalytic reactions. Recent studies point to electron charge donation from the support as the driving force to cleave the C=O bond in CO_2[61] or to enhance the reactivity through the anchors' electronic perturbation.[27,62] Therefore, the Ni dopants could affect the reactivity, acting as a potentially endless electron channel between the cluster and the Ni substrate.

3. Conclusion

We have shown that cobalt adatoms, dimers, and rather small nanoclusters (<3 nm diameter and 0.5 nm height) are stabilized at room temperature both on epitaxial graphene on Ni(111) and corrugated graphene on Ni(100). After annealing to 200 °C, clusters exhibit a well-defined and narrow size distribution. In addition, the clusters are stable on the graphene on Ni(100) support up to 250 °C. Carbon monoxide gas exposure up to 1×10^{-6} mbar does not influence the clusters size or shape, despite hints of an adsorption-desorption process promising for further investigation in catalytic conditions within this temperature and pressure range. The origin of this exceptional cluster stability can be traced back to an anchoring effect of single nickel atoms incorporated in the graphene network, as revealed by manipulation with the STM tip. In terms of stability, DFT calculations indicate that this anchoring effect is much stronger than the stabilizing effect of the moiré modulation, the method of choice to self-assemble nanostructures over the past two decades. The strong interaction of the graphene layer with the substrate on one hand and the highly active nucleation sites on the other hand result in the formation of cobalt clusters much smaller in size than reported so far. The size selectivity can be reasonably explained in terms of an optimal cluster size that balances competing
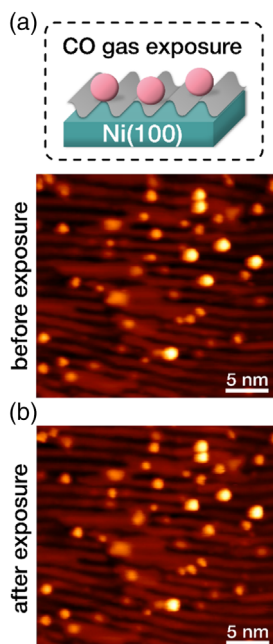
Figure 6. a) Co nanoclusters on G/Ni(100) before and b) after 1500 L CO gas exposure (up to 1×10^{-6} mbar partial pressure) show that no gas-induced mass-transport has taken place. (a: $I_t = 0.3$ nA, $V_b = -1.0$ V, b: $I_t = 0.3$ nA, $V_b = -1.0$ V).

ADVANCED
SCIENCE NEWS
www.advancedsciencenews.com

small
structures
www.small-structures.com

factors: the strong attractive effect of the anchor on the first atoms, the rather strong bulk cobalt cohesive energy, the rather weak cobalt–graphene interaction, the graphene-mediated repulsion between cobalt and the nickel surface. This peculiar template paves the way for a new class of metal nanostructured materials since low-cost polycrystalline nickel surfaces predominantly provide the crystal facets investigated here. The anchoring principle is likely to be easily transferrable for the design of size-selected clusters of various elements, to address the requirements of specific catalytic reactions.

4. Computational Details

The Quantum ESPRESSO suite was used to perform the DFT calculations.[63,64] G on Ni(100) surface was modeled using a supercell with a Ni slab of three layers and a 4×12 in-plane periodicity, similar to the one used in ref. [41]. The 3.52 Å lattice constant of Ni(100) matches with G strained 1.2% along the zig-zag direction, which coincides with the [011] crystal direction of the substrate. The effects of exchange and correlation were described using the PBE functional[65] and the van der Waals Grimme DF-D2 corrections were added to properly describe the G–Ni interaction.[66] We used the ultrasoft pseudopotentials from the Standard Solid State PPs library[67] and expanded the electron wave functions and density in a plane wave basis set with cutoff energies of 50 and 300 Ry, respectively. For structural relaxation, the Brillouin zone was sampled with the $2 \times 1 \times 1$ Γ-centered k-point mesh, whereas for the self-consistent field calculations, a denser $4 \times 1 \times 1$ mesh was used. During the structural relaxation, all atoms but those from the bottom Ni layer were allowed to move until all the forces dropped below 0.001 Ry Bohr^{-1}. The energy barriers for the diffusion processes of Co atoms on the surface were calculated using the NEB method.[68,69]

5. Experimental Section

Sample preparation and STM measurements were carried out in an ultra-high vacuum chamber with a base pressure of 1×10^{-10} mbar. Both the Ni(111) and Ni(100) crystals were cleaned, for each new preparation, by at least three cycles of sputtering (10–20 min, 9 μA, 2 keV, $p_{Ar+} = 2 \times 10^{-6}$ mbar) and annealing (10 min, 600 °C, 2 °C s^{-1} rate). For the G growth via chemical vapor deposition on Ni(100), the sample was cooled down to 500 °C during the last annealing cycle, and ethylene gas was dosed at $p = 5 \times 10^{-7}$ mbar for 90 min. The sample was kept for an additional 10 min at the growth temperature before cooling it down with a rather fast rate of 4 K s^{-1} to avoid carbide formation below 500 °C.[33,70] Low energy electron diffraction (LEED) measurements performed at sample temperatures below 100 °C show the absence of spots related to carbide, indicating a good quality G layer, as can be seen in Figure S1, Supporting Information. The same procedure was applied also to grow epitaxial G on Ni(111), except that the growth temperature was 560 °C, and a complete layer was obtained after 1 h of ethylene exposure. Co was evaporated by means of a specs electron beam evaporator (flux about 0.003 ML min^{-1}), yielding a nominal Co coverage of 0.03 ML after 10 min, as estimated from the STM images. STM measurements were performed in constant current mode with an Omicron VT-STM operated by a R9plus controller (RHK Technology). For the measurements of the temperature stability of Co clusters, the sample was annealed directly in the STM stage at about 1 K s^{-1} and stabilized at the desired temperature for about 5 min before proceeding with the measurements. The STM images were processed by means of the Gwyddion software.[71]

Supporting Information

Supporting Information is available from the Wiley Online Library or from the author.

Conflict of Interest

The authors declare no conflict of interest.

Data Availability Statement

The data that support the findings of this study are openly available in [Zenodo] at https://doi.org/10.5281/zenodo.8300878, reference number [8300878].

[1] C. Dong, Y. Li, D. Cheng, M. Zhang, J. Liu, Y. G. Wang, D. Xiao, D. Ma, *ACS Catal.* **2020**, *10*, 11011.

[2] B. Zhang, Y. Chen, J. Wang, H. Pan, W. Sun, *Adv. Funct. Mater.* **2022**, *32*, 2202227.

[3] S. Yang, G. Cui, S. Pang, Q. Cao, U. Kolb, X. Feng, J. Maier, K. Müllen, *ChemSusChem* **2010**, *3*, 236.

[4] C. Vo-Van, S. Schumacher, J. Coraux, V. Sessi, O. Fruchart, N. B. Brookes, P. Ohresser, T. Michely, *Appl. Phys. Lett.* **2011**, *99*, 142504.

[5] R. Xiao, D. Fritsch, M. D. Kuz, K. Koepernik, H. Eschrig, M. Richter, *Phys. Rev. Lett.* **2009**, *103*, 187201.

[6] T. Eelbo, M. Waśniowska, P. Thakur, M. Gyamfi, B. Sachs, T. O. Wehling, S. Forti, U. Starke, C. Tieg, A. I. Lichtenstein, R. Wiesendanger, *Phys. Rev. Lett.* **2013**, *110*, 136804.

[7] B. Böller, K. M. Durner, J. Wintterlin, *Nat. Catal.* **2019**, *2*, 1027.

[8] Y. Guo, M. Wang, Q. Zhu, D. Xiao, D. Ma, *Nat. Catal.* **2022**, *5*, 766.

[9] J. Yang, E. Z. Tveten, D. Chen, A. Holmen, *Langmuir* **2010**, *26*, 16558.

[10] A. Tuxen, S. Carenco, M. Chintapalli, C. H. Chuang, C. Escudero, E. Pach, P. Jiang, F. Borondics, B. Beberwyck, A. P. Alivisatos, G. Thornton, W. F. Pong, J. Guo, R. Perez, F. Besenbacher, M. Salmeron, *J. Am. Chem. Soc.* **2013**, *135*, 2273.

[11] A. Banerjee, V. Navarro, J. W. M. Frenken, A. P. Van Bavel, H. P. C. E. Kuipers, M. Saeys, *J. Phys. Chem. Lett.* **2016**, *7*, 1996.

[12] S. Yao, L. Lin, W. Liao, N. Rui, N. Li, Z. Liu, J. Cen, F. Zhang, X. Li, L. Song, L. Betancourt De Leon, D. Su, S. D. Senanayake, P. Liu, D. Ma, J. G. Chen, J. A. Rodriguez, *ACS Catal.* **2019**, *9*, 9087.

[13] B. Eren, D. Zherebetskyy, L. L. Patera, C. H. Wu, H. Bluhm, C. Africh, L. W. Wang, G. A. Somorjai, M. Salmeron, *Science* **2016**, *351*, 475.

[14] H. Rong, S. Ji, J. Zhang, D. Wang, Y. Li, *Nat. Commun.* **2020**, *11*, 5884.

[15] V. Chesnyak, S. Stavrić, M. Panighel, G. Comelli, M. Peressi, C. Africh, *Nanoscale* **2022**, *14*, 3589.

[16] Y. Chen, J. Wei, M. S. Duyar, V. V. Ordomsky, A. Y. Khodakov, J. Liu, *Chem. Soc. Rev.* **2021**, *50*, 2337.

[17] Z. Hajjar, M. Doroudian Rad, S. Soltanali, *Res. Chem. Intermed.* **2017**, *43*, 1341.

[18] W. Luo, S. Zafeiratos, *ChemPhysChem* **2016**, *17*, 3055.

[19] A. T. N'Diaye, T. Gerber, C. Busse, J. Myslivček, J. Coraux, T. Michely, *New J. Phys.* **2009**, *11*, 103045.

[20] F. Loi, M. Pozzo, L. Sbuelz, L. Bignardi, P. Lacovig, E. Tosi, S. Lizzit, A. Kartouzian, U. Heiz, R. Larciprete, D. Alfè, A. Baraldi, *Appl. Surf. Sci.* **2023**, *619*, 156755.

[21] A. T. N'Diaye, S. Bleikamp, P. J. Feibelman, T. Michely, *Phys. Rev. Lett.* **2006**, *97*, 215501.

[22] A. J. Martínez-Galera, U. A. Schröder, C. Herbig, M. A. Arman, J. Knudsen, T. Michely, *Nanoscale* **2017**, *9*, 13618.

[23] L. Wang, S. Ma, Z. Jiao, D. Yuan, *Appl. Surf. Sci.* **2019**, *465*, 1.

[24] C. Jin, L. Cheng, G. Feng, R. Ye, Z. H. Lu, R. Zhang, X. Yu, *Langmuir* **2022**, *38*, 3694.

[25] S. Sahoo, M. E. Gruner, S. N. Khanna, P. Entel, *J. Chem. Phys.* **2014**, *141*, 074707.

[26] F. Montejo-Alvaro, H. M. Alfaro-López, M. G. Salinas-Juárez, H. Rojas-Chávez, M. S. Peralta-González, F. J. Mondaca-Espinoza, H. Cruz-Martínez, *J. Nanopart. Res.* **2023**, *25*, 11.

[27] Y. R. Wang, L. F. Wang, S. H. Ma, *Appl. Surf. Sci.* **2019**, *481*, 1080.

[28] M. Farnesi Camellone, F. Dvořák, M. Vorokhta, A. Tovt, I. Khalakhan, V. Johánek, T. Skála, I. Matolínová, S. Fabris, J. Myslivček, *ACS Catal.* **2022**, *12*, 4859.

[29] Z. Zou, V. Carnevali, M. Jugovac, L. L. Patera, A. Sala, M. Panighel, C. Cepek, G. Soldano, M. M. Mariscal, M. Peressi, G. Comelli, C. Africh, *Carbon* **2018**, *130*, 441.

[30] F. Bianchini, L. L. Patera, M. Peressi, C. Africh, G. Comelli, *J. Phys. Chem. Lett.* **2014**, *5*, 467.

[31] Z. Zou, L. L. Patera, G. Comelli, C. Africh, *J. Phys. Chem. C* **2020**, *124*, 25308.

[32] Z. Zou, L. L. Patera, C. Africh, *Carbon* **2021**, *172*, 296.

[33] L. L. Patera, C. Africh, R. S. Weatherup, R. Blume, S. Bhardwaj, C. Castellarin-Cudia, A. Knop-Gericke, R. Schloegl, G. Comelli, S. Hofmann, C. Cepek, *ACS Nano* **2013**, *7*, 7901.

[34] V. Carnevali, L. L. Patera, G. Prandini, M. Jugovac, S. Modesti, G. Comelli, M. Peressi, C. Africh, *Nanoscale* **2019**, *11*, 10358.

[35] Z. Zhou, F. Gao, D. W. Goodman, *Surf. Sci.* **2010**, *604*, L31.

[36] S. W. Poon, A. T. S. Wee, E. S. Tok, *Surf. Sci.* **2012**, *606*, 1586.

[37] L. H. De Lima, R. Landers, A. De Siervo, *Chem. Mater.* **2014**, *26*, 4172.

[38] Q. Liao, H. J. Zhang, K. Wu, H. Y. Li, S. N. Bao, P. He, *Nanotechnology* **2011**, *22*, 125303.

[39] A. Baby, L. Trovato, C. Di Valentin, *Carbon* **2021**, *174*, 772.

[40] X. Liu, Y. Han, J. W. Evans, A. K. Engstfeld, R. J. Behm, M. C. Tringides, M. Hupalo, H. Q. Lin, L. Huang, K. M. Ho, D. Appy, P. A. Thiel, C. Z. Wang, *Prog. Surf. Sci.* **2015**, *90*, 397.

[41] S. Stavrić, V. Chesnyak, S. del Puppo, M. Panighel, G. Comelli, C. Africh, Ž. Šljivančanin, M. Peressi, *Carbon* **2023**, *215*, 118486.

[42] K. Zhao, N. Janulaitis, J. R. Rumptz, C. T. Campbell, *ACS Catal.* **2023**, *13*, 2670.

[43] R. T. Frederick, Z. Novotny, F. P. Netzer, G. S. Herman, Z. Dohnálek, *J. Phys. Chem. B* **2018**, *122*, 640.

[44] L. Huang, Y. Pan, L. Pan, M. Gao, W. Xu, Y. Que, H. Zhou, Y. Wang, S. Du, H. J. Gao, *Appl. Phys. Lett.* **2011**, *99*, 163107.

[45] N. Podda, M. Corva, F. Mohamed, Z. Feng, C. Dri, F. Dvořák, V. Matolin, G. Comelli, M. Peressi, E. Vesselli, *ACS Nano* **2017**, *11*, 1041.

[46] T. Gerber, E. Granäs, U. A. Schröder, P. Stratmann, K. Schulte, J. N. Andersen, J. Knudsen, T. Michely, *J. Phys. Chem. C* **2016**, *120*, 26290.

[47] G. S. Parkinson, Z. Novotny, G. Argentero, M. Schmid, J. Pavelec, R. Kosak, P. Blaha, U. Diebold, *Nat. Mater.* **2013**, *12*, 724.

[48] L. Xu, M. Papanikolaou, K. G. J. Lechner, B. A. Je, L. Somorjai, G. A. Salmeron, M. Mavrikakis, *Science* **2023**, *380*, 70.

[49] M. Ma, Z. Huang, D. E. Doronkin, W. Fa, Z. Rao, *Appl. Catal., B* **2022**, *300*, 120695.

[50] M. Ehrensperger, J. Wintterlin, *J. Catal.* **2014**, *319*, 274.

[51] V. Chesnyak, M. Panighel, M. Tallone, S. Stavrić, D. Povoledo, S. Del Puppo, M. Peressi, G. Comelli, C. Africh, *Data set. Zenodo* **2023**, https://doi.org/10.5281/zenodo.8300878.

[52] C. J. Weststrate, P. Van Helden, J. Van De Loosdrecht, J. W. Niemantsverdriet, *Surf. Sci.* **2016**, *648*, 60.

[53] H. Wang, W. Zhou, J. X. Liu, R. Si, G. Sun, M. Q. Zhong, H. Y. Su, H. B. Zhao, J. A. Rodriguez, S. J. Pennycook, J. C. Idrobo, W. X. Li, Y. Kou, D. Ma, *J. Am. Chem. Soc.* **2013**, *135*, 4149.

[54] G. Malaet, W. T. Ralston, C.-S. Li, S. Alayoglu, K. An, N. Musselwhite, B. Kalkan, G. A. Somorjai, *J. Am. Chem. Soc.* **2014**, *136*, 2260.

[55] S. Karimi, A. Tavasoli, Y. Mortazavi, A. Karimi, *Appl. Catal., A* **2015**, *499*, 188.

[56] L. Wang, L. Wang, J. Zhang, X. Liu, H. Wang, W. Zhang, Q. Yang, J. Ma, X. Dong, S. J. Yoo, J. G. Kim, X. Meng, F. S. Xiao, *Angew. Chem., Int. Ed.* **2018**, *57*, 6104.

[57] T. Fan, H. Liu, S. Shao, Y. Gong, G. Li, Z. Tang, *J. Phys. Chem. Lett.* **2021**, *12*, 10486.

[58] S. Lee, A. Halder, G. A. Ferguson, S. Seifert, R. E. Winans, D. Teschner, R. Schlögl, V. Papaefthimiou, J. Greeley, L. A. Curtiss, S. Vajda, *Nat. Commun.* **2019**, *10*, 954.

[59] J. P. Den Breejen, P. B. Radstake, G. L. Bezemer, J. H. Bitter, V. Frøseth, A. Holmen, K. P. De Jong, *J. Am. Chem. Soc.* **2009**, *131*, 7197.

[60] L. Fang, S. Seifert, R. E. Winans, T. Li, *Small Methods* **2021**, *5*, 2001194.

[61] P. López-Caballero, A. W. Hauser, M. Pilar De Lara-Castells, *J. Phys. Chem. C* **2019**, *123*, 23064.

[62] A. Zitolo, V. Goellner, V. Armel, M. T. Sougrati, T. Mineva, L. Stievano, E. Fonda, F. Jaouen, *Nat. Mater.* **2015**, *14*, 937.

[63] P. Giannozzi, S. Baroni, N. Bonini, M. R. Car, C. Cavazzoni, D. Ceresoli, G. L. Chiarotti, M. Cococcioni, I. Dabo, A. Dal Corso, S. De Gironcoli, S. Fabris, G. Fratesi, R. Gebauer, U. Gerstmann, C. Gougoussis, A. Kokalj, M. Lazzeri, L. Martin-Samos, N. Marzari, F. Mauri, R. Mazzarello, S. Paolini, A. Pasquarello, L. Paulatto, C. Sbraccia, S., G. Sclauzero, A. P. Seitsonen, et al., *J. Phys.: Condens. Matter* **2009**, *21*, 395502.

[64] P. Giannozzi, O. Andreussi, T. Brumme, O. Bunau, M. Buongiorno Nardelli, M. , R. Car, C. Cavazzoni, D. Ceresoli, M. Cococcioni,

N. Colonna, I. Carnimeo, A. Dal Corso, S. de Gironcoli, P. Delugas, R. A. DiStasio, A. Ferretti, A. Floris, G. Fratesi, G. Fugallo, R. Gebauer, U. Gerstmann, F. Giustino, T. Gorni, J. Jia, M. Kawamura, H.-Y. Ko, A. Kokalj, E. Küçükbenli, M. Lazzeri, et al., *J. Phys.: Condens. Matter* **2017**, *29*, 465901.

[65] J. P. Perdew, K. Burke, M. Ernzerhof, *Phys. Rev. Lett.* **1996**, *77*, 3865.

[66] S. Grimme, *J. Comput. Chem.* **2006**, *27*, 17487.

[67] G. Prandini, A. Marrazzo, I. E. Castelli, N. Mounet, N. Marzari, *npj Comput. Mater.* **2018**, *4*, 72.

[68] G. Henkelman, B. P. Uberuaga, H. Jónsson, *J. Chem. Phys.* **2000**, *113*, 9901.

[69] G. Henkelman, H. Jónsson, *J. Chem. Phys.* **2000**, *113*, 9978.

[70] S. Stavrić, S. del Puppo, Ž. Šljivančanin, M. Peressi, *Phys. Rev. Mater.* **2021**, *5*, 014003.

[71] D. Nečas, P. Klapetek, *Cent. Eur. J. Phys.* **2012**, *10*, 181.